Physica Medica 104 (2022) 75–84

Contents lists available at ScienceDirect

Physica Medica

journal homepage: www.elsevier.com/locate/ejmp

Technical note

The use of cardiac CT acquisition mode for dynamic musculoskeletal imaging

Benyameen Keelson [a,b,d,*], Luca Buzzatti [e], Gert Van Gompel [a], Thierry Scheerlinck [c], Savanah Hereus [e], Johan de Mey [a], Erik Cattrysse [e], Jef Vandemeulebroucke [b,d], Nico Buls [a]

[a] Vrije Universiteit Brussel (VUB), Universitair Ziekenhuis Brussels (UZB), Department of radiology, Laarbeeklaan 101, 1090 Brussels, Belgium
[b] Vrije Universiteit Brussel (VUB), Department of Electronics and Informatics (ETRO), Pleinlaan 9, 1050 Brussels, Belgium
[c] Vrije Universiteit Brussel (VUB), Universitair Ziekenhuis Brussel (UZ Brussel), Department of Orthopaedic Surgery and Traumatology, Laarbeeklaan 101, 1090 Brussels, Belgium
[d] IMEC, Kapeldreef 75, B-3002 Leuven, Belgium
[e] Vrije Universiteit Brussel (VUB) Department of Physiotherapy, Human Physiology and Anatomy, Laarbeeklaan 103, 1090 Brussels, Belgium

ARTICLE INFO

Keywords:
Dynamic Computed Tomography
Musculoskeletal imaging
Motion artifacts
Cardiac mode
Phantom study

ABSTRACT

Objectives: To quantitatively evaluate the impact of a cardiac acquisition CT mode on motion artifacts in comparison to a conventional cine mode for dynamic musculoskeletal (MSK) imaging.
Methods: A rotating PMMA phantom with air-filled holes drilled at varying distances from the disk center corresponding to linear hole speeds of 0.75 cm/s, 2.0 cm/s, and 3.6 cm/s was designed. Dynamic scans were obtained in cardiac and cine modes while the phantom was rotating at 48°/s in the CT scanner. An automated workflow to compute the Jaccard distance (JD) was established to quantify degree of motion artifacts in the reconstructed phantom images. JD values between the cardiac and cine scan modes were compared using a paired sample *t*-test. In addition, three healthy volunteers were scanned with both modes during a cyclic flexion–extension motion of the knee and analysed using the proposed metric.
Results: For all hole sizes and speeds, the cardiac scan mode had significantly lower (p-value <0.001) JD values. (0.39 [0.32–0.46]) i.e less motion artifacts in comparison to the cine mode (0.72 [0.68–0.76]). For both modes, a progressive increase in JD was also observed as the linear speed of the holes increased from 0.75 cm/s to 3.6 cm/s. The dynamic images of the three healthy volunteers showed less artifacts when scanned in cardiac mode compared to cine mode, and this was quantitatively confirmed by the JD values.
Conclusions: A cardiac scan mode could be used to study dynamic musculoskeletal phenomena especially of fast-moving joints since it significantly minimized motion artifacts.

Introduction

There is a growing interest in using wide beam CT's for imaging dynamic phenomena of musculoskeletal (MSK) pathologies in what is known as 4D-CT MSK imaging (3D + time) [1]. For instance, patella instability during knee movement has been investigated for both symptomatic and asymptomatic sides by means of 4D-CT [2,3]. Other studies have also investigated different joint pathologies of the wrist, hip and foot by means of 4D-CT [4–6]. In addition, Buzzatti et al. [7] used 4D-CT to investigate the feasibility of detecting changes in kinematics after sequentially sectioning lateral collateral ligaments of one fresh frozen cadaver foot. This technique leverages the wide craniocaudal volume coverage (z-axis collimation up to 16 cm) of modern wide-beam CT scanners combined with fast tube rotation speeds (down to 0.22 s) to produce functional and morphological information of joints at high temporal and spatial resolutions.

The approaches used to achieve 4D-CT MSK imaging vary from study to study especially in how the dynamic images are obtained. Some studies make use of single source CT scans to repeatedly scan a structure that is undergoing motion without table movement in what is termed cine mode acquisition [6,8,9]. With the predominant parameter in 4D-CT MSK imaging being the temporal resolution, some studies have

* Corresponding author at: Department of Radiology, Universitair ziekenhuis Brussel (UZB), Vrije Universiteit Brussel (VUB), Laarbeeklaan 101, 1090 Brussel, Belgium.
E-mail addresses: bkeelson@etrovub.be, benyameen.keelson@vub.be (B. Keelson).

https://doi.org/10.1016/j.ejmp.2022.10.028
Received 17 June 2022; Received in revised form 30 September 2022; Accepted 31 October 2022
Available online 10 November 2022

used dual source CT (DSCT) systems [10,11] which allow to cut temporal resolution by half compared to a single source CT system of the same tube rotation time. Such DSCT systems are useful in analysis of smaller joints such as the wrist but are not capable of capturing motion of larger joints such as the hip, knee, and ankle. This is because most of these systems do not have 16 cm z-axis coverage and require table movement to capture whole structures.

Further improvement in temporal resolution, however, has an upper limit since faster gantry rotation times come along significant technical challenges. 4D-CT MSK applications bring forth new challenges, as the structures are purposefully undergoing movement. An equally important factor to consider in 4D-CT imaging are motion artifacts which result from inconsistent views in the projection data. Motion artifacts result in blurring or apparent doubling of structures in the reconstructed images which translates into shape distortions and/or uncertainties in structure localisation. In most dynamic MSK imaging applications, the motion of individual bones is of prime interest for extracting kinematic parameters. This is usually achieved by means of image processing techniques such as image registration, if needed accompanied by prior object segmentation [12]. The presence of shape distortions in the reconstructed image resulting from motion artifacts therefore have an influence on the localization of structures in the registration step and impede reliable motion estimation from dynamic MSK images.

Approaches to mitigate these artifacts is therefore essential for the clinical introduction of 4D-CT MSK applications. Teixera et al. [13] conducted experiments with a rotating phantom and correlated their data with a cadaver study to provide evidence-based recommendations for 4D-CT MSK applications. Their study used tube rotation times of 0.35 s and 0.5 s and had two radiologists review and grade motion artifacts in the reconstructed images.

The technical demands necessary for cardiac CT imaging makes systems designed for such applications suitable for obtaining images of coronary arteries with significantly lower motion artifacts. This is achieved by means of innovative reconstruction techniques [14–16]. In the work of Leng et al., [10] a cardiac scan mode on a dual source CT was used to obtain MSK imaging of a cadaver wrist. Neo et al [11] also used a cardiac scan mode to investigate the effect of motion velocity on image quality for dynamic carpal imaging applications. Both studies were conducted on 64 slice systems and focused on scanning smaller joints like the wrist.

To the best of our knowledge, no studies have been conducted on the use of the cardiac scan mode in acquiring dynamic images from larger joints such as the knee. Unlike cardiac motion, MSK motion is not periodical and can show larger translations and rotations between successive time points. It is therefore important to quantitatively investigate the benefit of a cardiac reconstruction mode for such applications and how it compares to cine mode acquisitions.

Conventional image quality metrics such as SNR and CNR alone may not capture the unique nature of motion artifacts. In a previous study, a basic customized thresholding approach based on sampling intensities from concentric circles on an air-filled rotating PMMA phantom was used to compare motion artifacts between a cardiac acquisition and conventional acquisition mode on selected slices from a single time point [17]. This approach however required manual steps and did not consider the effect of motion artifacts from other time points. This is essential since motion artifacts can vary within the different time points of a dynamic CT acquisition,

In this current study, we leverage the benefits of the cardiac mode and investigate its extension to dynamic MSK imaging applications. We propose a generic custom automated processing workflow based on image registration and segmentation to enable quantifying motion artifacts from different time points of a rotating phantom motion. This approach aims to evaluate distortions in shape and structure, and the impact of the phantom rotation on the quality of the images. The aim was to quantitatively compare dynamic scans of the phantom obtained in cine mode to those obtained using the cardiac mode. Furthermore, in a clinical study, dynamic scans of knee joints during a cyclic flexion extension motion were also obtained in both cardiac and cine modes, to verify the findings from the phantom experiments.

Materials and methods

Phantom

The rotating phantom consisted of a polymethylmethacrylate (PMMA) disk (70 mm radius) with 9 mm-deep air-filled holes of varying radii (1 mm, 2 mm and 3 mm). The holes were drilled in pairs at 9 mm, 24 mm, 44 mm, and 64 mm from the disk center. This allowed to observe hole pairs at different linear speeds. The individual holes were spaced out at 2 mm for the 1 mm holes, 4 mm for the 2 mm holes, and 6 mm for the 3 mm holes [Fig. 1]. A Trinamic 24 V electric motor (TRINAMIC Motion Control Hamburg, Germany) was used to rotate the phantom and an Arduino uno board (Arduino AG) controlled the motor speed.

Dynamic CT acquisitions

Dynamic CT images were acquired on a clinical single source 256-slice Revolution CT (GE Healthcare, Waukesha, Wisconsin, USA). Similar scan settings were used for both cardiac and cine acquisitions. Tube voltage was 120 kVp, tube current was kept constant at 150 mA and gantry rotation time was 0.28 s. The phantom was positioned in the isocenter and rotated at 48°/s in the same axis as the gantry for all dynamic acquisitions. This corresponded to linear hole speeds of 0.75 cm/s, 2.0 cm/s, and 3.6 cm/s in relation to the distance of each hole to the disk center. These hole speeds reflected speed of motions previously observed during experiments of ankle, knee and elbow movements [18,19].

Both scan modes were implemented to have similar scan durations (6 s). This is essential in dynamic MSK imaging since a subject must perform a motion in an ample amount of time. To achieve this for cardiac mode, retrospective ECG-gated cardiac CT imaging where data was constantly obtained (without table motion) throughout a simulated cardiac cycle (0 to 300 % representing 3 cardiac cycles) was used. The ECG signal, was simulated at the lowest heart rate available of 30 bpm allowing for the scan duration of 6 s. The dynamic sequences were obtained by reconstructing images over the 6 s scan duration. Fig. 2 presents an illustration of the cardiac mode acquisition.

Scans in cine mode were obtained by repeated scans without table motion while the phantom rotated. The number of repeated scans is determined by the *number of passes* parameter which was set to 21 to ensure a similar total scan duration of about 6 secs. The *time-between-images* was set to 0.14 s. This parameter determines the interval at which successive images following the first 0.28 s rotation are updated. This resulted in a series of volumetric CT images depicting the phantom at different stages of motion.

All images were reconstructed using adaptive statistical iterative reconstruction (ASIR 50 %), with pixel size 0.298 mm and slice thickness 0.625 mm with a 320 mm field of view. Experiments were repeated three times for each scan mode. For each scan mode, an image of the phantom in a stationary state was obtained (static image) which served as the ground truth to which corresponding dynamic images were compared.

Motion artifact quantification

A quantification of the motion artifact was obtained by computing the Jaccard distance [Eqn. (1)] of hole segmentations in the static phantom (no motion artifacts) with corresponding segmentations in the dynamic phantom images (with motion artifacts). The static and dynamic images were initially spatially aligned by a pairwise 3D rigid registration using a two-step approach developed in python with the open-source software simpleITK [20]. Firstly, corresponding points were

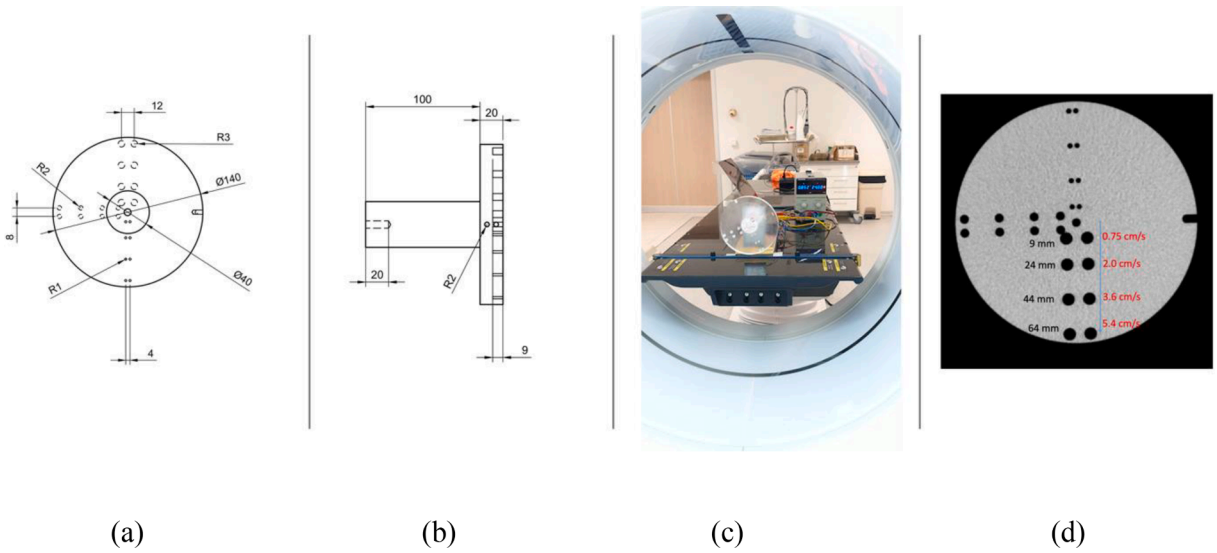

Fig. 1. Figure showing the dimensions used for the design of the phantom, its setup in the CT gantry and a static image of the phantom. Number inserts on static phantom show the distance from the disk center to each hole center (black text) and their corresponding linear speeds (red text) for a phantom rotation speed of 48°/s.

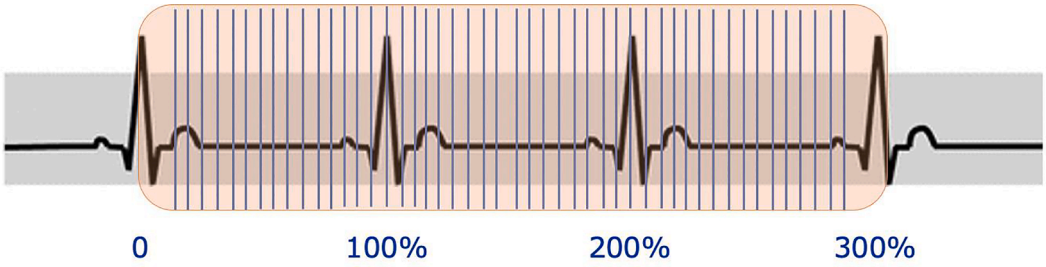

Fig. 2. The figure shows a representative drawing of the principle used in creating dynamic sequences for the cardiac mode. A schematic ECG signal over 3 cardiac cycles (0–300%) is shown. Shaded area is an indication of constant data acquisition over the entire cardiac cycles. Blue lines are an indication of the reconstructions at a chosen interval to create the dynamic sequences. For the phantom study reconstructions were done from 0 to 150% at 5% intervals, for the knee data reconstructions were obtained over the entire 0–300% at 2% intervals.

automatically computed between the static position and each of the dynamic positions using scale invariant feature transformation (SIFT) [21]. The detected corresponding points were then used in a multi metric rigid pairwise registration step. The registration minimizes both the distance between points on the static position and the corresponding points on the dynamic images as well as the mean square difference between the image intensities.

The metric was evaluated on automatically detected regions of interest (ROIs) corresponding to the different hole pair positions. Fig. 3 gives an overview of the workflow on one of the holes for the static, cine, and cardiac images.

A threshold of −400 HU was selected based on the histogram of the static phantom image [Fig. 8a] and applied on both the static and the dynamic images. A binary image representing voxels below −400 HU (holes) was then obtained for both static and dynamic images of the two CT acquisition modes. The degree of motion artifact was then defined as the measure of dissimilarity between static phantom hole segmentations and the dynamic image hole segmentations:

$$\textit{Jaccard distance}[\mathbf{0},\mathbf{1}] = \mathbf{1} - \boldsymbol{J}(\boldsymbol{A},\boldsymbol{B}), \tag{1}$$

$$\boldsymbol{J}(\boldsymbol{A},\boldsymbol{B}) = \frac{|\boldsymbol{A} \cap \boldsymbol{B}|}{|\boldsymbol{AUB}|}, \tag{2}$$

where **J (A,B)** is the Jaccard index [22], ***A*** is the binary image of hole segmentations in the static phantom and ***B*** is the binary image of hole segmentations in the dynamic images. A value of 0 indicates a ROI with no motion artifacts and 1 a region with severe motion artifacts. The metric takes into consideration contour abnormalities (distortions, ghosting and blurring) as well as alterations in the number of visible holes in the reconstructed images. The metric was evaluated as a function of hole radii (1 mm, 2 mm, 3 mm) and linear speeds (0.75 cm/s, 2.0 cm/s and 3.6 cm/s) based on the hole distance from the disk center. Results were averaged over the different time points and over the three experiment repetitions. In addition, the distribution of the pixel intensities in the ROI's were also presented as histograms. The contrast to noise ratio (CNR) was also computed as the ratio of the difference in signal intensity between ROIs in air and background (PMMA) to the noise in the background ROI. The ROIs were purposefully placed adjacent to each other (Fig. 8), to capture discrepancies in intensity and noise introduced by the motion artifact.

Data distribution was checked using Shapiro-Wilk test for normality

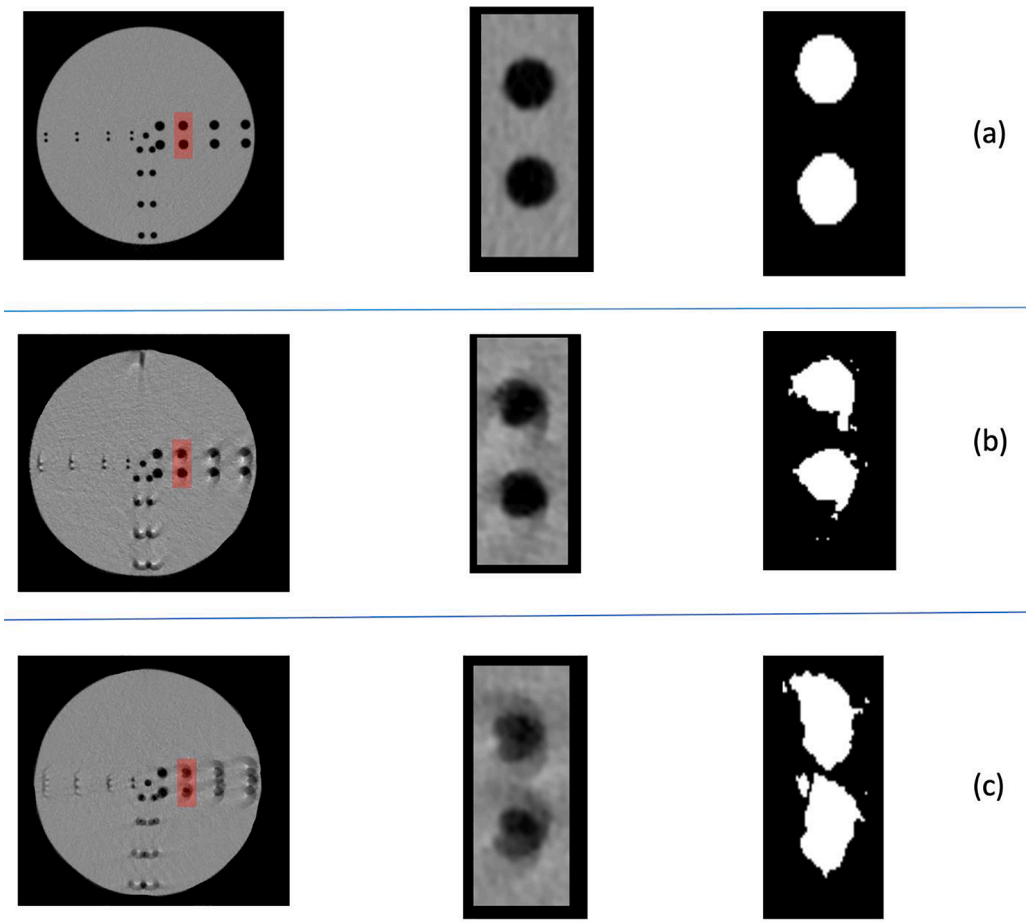

Fig. 3. The figure shows the workflow from ROI extraction to segmentation of the holes in the ROI for the static (a), cardiac (b) and cine (c) scans.

[23] A paired sample *t*-test was used in the comparison of normally distributed data. A Wilcoxon signed-ranks test [24] was performed for the pooled data of all speeds ($p = 0.05$).

Dynamic acquisitions of the knee

Three volunteers were scanned with both the cine and cardiac modes after having signed written informed consent. The participants were part of a lager study on dynamic CT of lower extremities which received ethical approval from our institution's ethics committee (B.U.N 143201733617). Participants were instructed to perform cyclic flexion/extension motion of both knees on a customized wooden bed support [Fig. 4]. A metronome at 25 bpm provided the pace of the motion and ensured all three subjects maintained an approximate constant movement. Scan parameters for these acquisitions were 80 kV tube voltage, 0.28 s gantry speed and tube current 50 mA for both scan modes. $CTDI_{vol}$ was 6.50 mGy for the cine acquisitions and 6.74 mGy for the cardiac mode acquisitions. The images for both modes were reconstructed with slice widths 0.977 mm × 0.977 mm and 2.5 mm slice thickness without any motion correction algorithm. Effective dose was calculated using the National Cancer Institute dosimetry system for CT. [25]. Similar to the phantom experiments, we computed the Jaccard distance for both scan modes. A pairwise 3D rigid registration between the static image and dynamic images was obtained with focus on the largest bone in the view (femur). This bone was then segmented by thresholding on both the static images and the registered dynamic images. The choice of threshold for these experiments was 400 HU chosen to capture high intensity voxels of bone [26,27].

Fig. 4. The figure shows the cyclic flexion–extension movement training session of one of the participants. The end motions, flexion (a) and extension (b) are shown in this image.

Results

Phantom study

The two-step registration approach successfully registered each of the dynamic sequences to the corresponding static phantom. An example of the registration result between static and one of the moving images is shown in Fig. 5.

Table 1 summarizes the Jaccard distance values for the cine and cardiac scans at comparable hole speeds. Significant differences in favour of the cardiac mode were observed for all individual speeds.

The box plots in Fig. 6. show the metric as a function of hole size and hole speed for the two CT acquisition modes.

The difference between the two scan modes was also observed visually on the reconstructed images [Fig. 7]. The distribution of pixel intensities in the region of interest for the static phantom compared to the dynamic images obtained in cardiac and cine modes are shown in Fig. 8. Differences in the histograms are highlighted on the figure.

Dynamic acquisitions of the knee

Slices from reconstructed images of the dynamic scans of the knee acquired in cardiac and cine modes are shown in Fig. 9. Motion artifacts are prominent on the cine scans as duplicated bones. Fig. 10 also shows how the motion artifact varies from time point within the same acquisition. Mean Jaccard distance values were significantly lower for the cardiac mode than in cine mode for all three volunteers ($p = 0.018$, $p = 0.043$, $p = 0.028$) respectively (Fig. 11). The effective dose for each of the scans was estimated to be 0.02 mSv for both cine and cardiac modes.

Discussion and conclusion

In this study, a custom-made rotating phantom was used to investigate the impact of a cardiac scan mode compared to a cine scan mode on motion artifacts for the purpose of MSK dynamic CT studies. We proposed an automated workflow to quantify the degree of motion artifacts in the reconstructed phantom images by computing the Jaccard distance between the static phantom images and corresponding dynamic images. The differences in motion artifact of the scan modes were also demonstrated visually on dynamic images of the knee in three healthy volunteers during a flexion–extension movement. The cardiac scan mode showed significantly lower ($p < 0.001$) Jaccard distance values 0.39 [0.32–0.46] in comparison to the cine mode 0.72 [0.68–0.76] at linear speeds of 3.6 cm/s. In both cine and cardiac modes, a progressive decline was observed in the quality of images as the speed of the holes increased from 0.75 cm/s to 3.6 cm/s. This is in accordance with the work of Teixera et al where they observed excessive motion artifacts were frequently located where linear speeds are higher. [12] ROI's for computing CNR in the phantom were positioned close to each other to capture the effect of the motion artifacts. Clinical placements of ROI's in the dynamic MSK images might however not be reproducible and fail to fully capture the effect of the motion artifacts and justify the need for an adapted metric to quantify such artifacts.

Table 1
Jaccard distance as a measure of motion artifacts for cardiac and cine CT scan modes at different linear speeds.

Hole speed cm/s	Cardiac scan mode Jaccard distance mean [95 % CI]*	Cine scan mode Jaccard distance mean [95 % CI]*	p-value
0.75	0.10 [0.09–0.11]	0.12 [0.11–0.13]	$p < 0.001$
2.0	0.22 [0.17–0.27]	0.50 [0.42–0.58]	$p < 0.001$
3.6	0.39 [0.32–0.46]	0.72 [0.68–0.76]	$p < 0.001$

*Results shown are for all hole radii and averaged over the dynamic sequence and the three repetitions.

The observed differences between scan modes in the phantom experiments were corroborated on clinical images of the three healthy volunteers during a flexion–extension motion of the knee. Blurring artifacts and doubling of bones were more apparent on the reconstructed images obtained in cine mode for all three subjects and was quantitatively confirmed by the JD values. Such artifacts can hinder diagnosis as well as any further image processing steps which are essential in providing quantitative kinematic analysis.

CT Imaging of joints has previously been driven by static images which are helpful in identifying morphological changes or fractures. However, a shift towards dynamic and functional imaging is important since certain MSK pathologies can be limited to a particular maneuver or motion path. For instance, abnormal motion of the patella has been found to be present in the first 30 degrees of knee flexion at the moment where the patella engages the trochlea [28]. In addition, abrupt abnormal motion of the first carpal row during radio-ulnar deviation has been reported in literature [29].

Dynamic CT offers the opportunity to obtain volumetric and intra-articular information of bones during physiologic motion. It allows physicians to gain diagnostic insights based on the qualitative evaluation of joint motion. Furthermore, subtle dynamic instabilities can be quantitatively assessed by means of image processing procedures and computations, such as image segmentation and registration. However, these processing techniques can be sensitive to the presence of motion artifacts and hinder any automated workflow for extracting quantitative kinematic parameters. Hence, for this technique to gain clinical popularity, there is the need to explore the optimal scan modes to provide quality images at reasonable radiation burden to the patient.

In this study, both cardiac and cine acquisitions were performed with

Fig. 5. The figure shows overlays of the moving phantom (green) and the static phantom (magenta) before (a) and after the registration step (b).

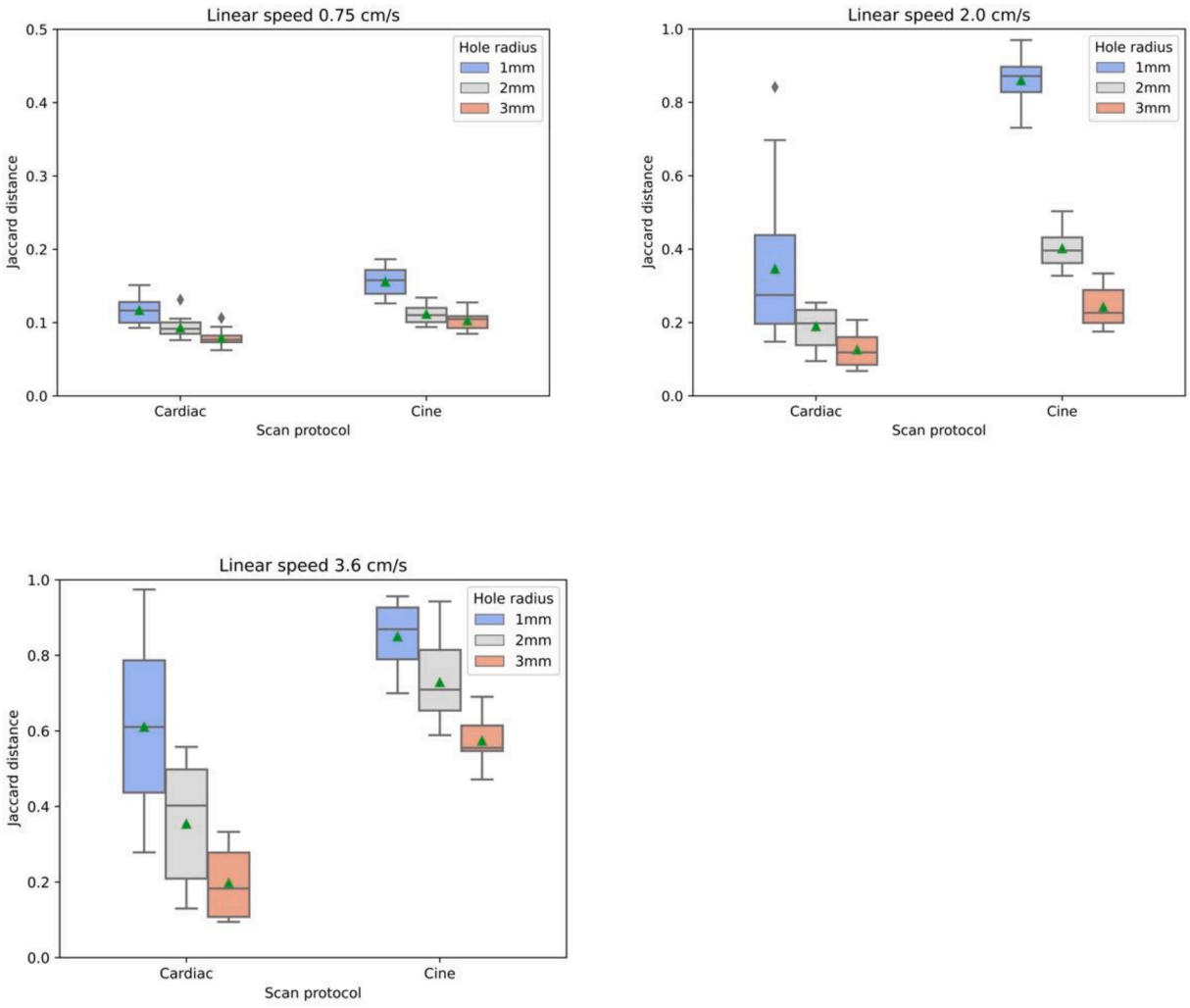

Fig. 6. Box plots showing the distribution of the Jaccard distance (0 representing no motion artifacts, 1 representing severe motion artifacts) of the two dynamic CT acquisition modes for different hole radii (1 mm,2 mm and 3 mm) at 0.75 cm/s, 2.0 cm/s and 3.6 cm/s. The results here are from all time points and for the three repetitions. The boxes show the interquartile range (IQR), vertical lines represent the median, the whiskers extend to the extreme data points within ± 1.5 IQR of the median. The mean values are displayed as green arrow heads.

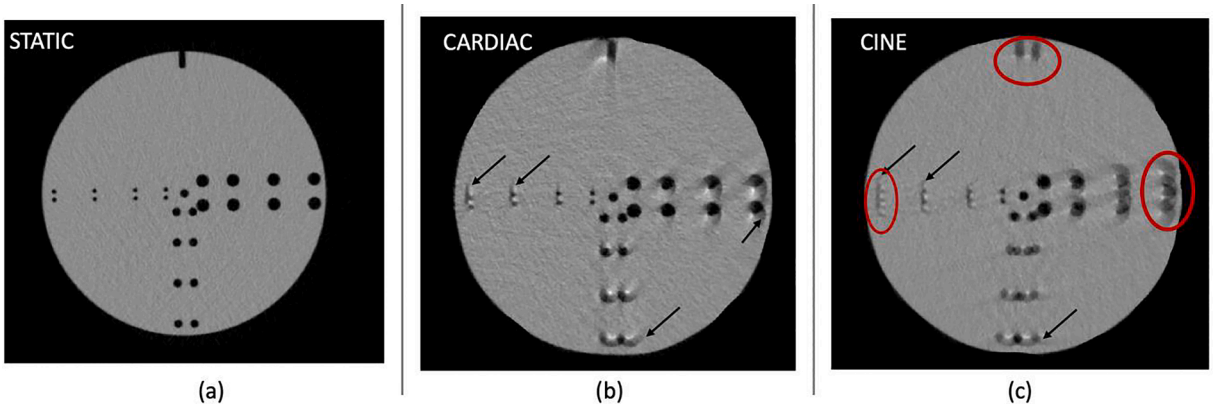

Fig. 7. The figure shows the differences in motion artifacts between the cardiac (b) and cine scan mode (c) as compared to the static phantom (a). Red ellipses highlight the duplication of holes (ghosting) and black arrows show blurring and distortion of holes. Notice how the cardiac mode reconstructions does not have duplicated holes even at the highest hole speeds.

the same tube voltage, tube current and tube rotation time. Hence the $CTDI_{vol}$ and effective dose values were similar. However, the cardiac scan mode on the system used in this study was limited to three cardiac cycles. A consequence of this is that acquisitions can only be obtained within a short time window of about 6 s when the lowest heartbeat of 30 bpm is simulated. Such a scan duration might not be long enough in

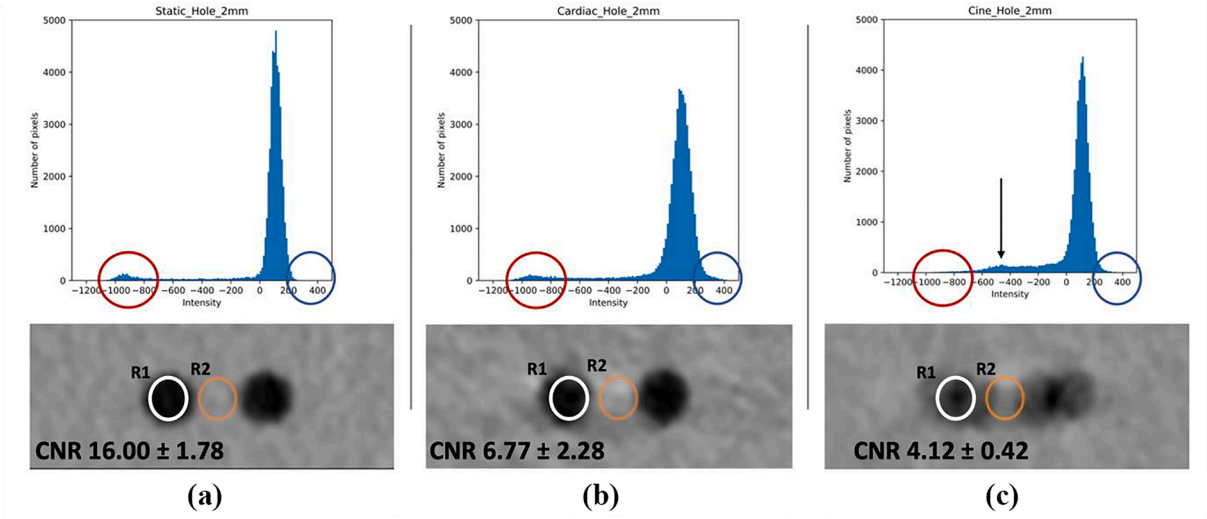

Fig. 8. The figure shows the histograms and CNR values (mean ± sd) of the static phantom image (a) in comparison to moving phantom images obtained in cardiac (b) and cine mode (c) for a 2 mm hole size at 2 cm/s hole speed. The red circles highlight low intensities representing the holes. Notice how these intensities are missing in the cine mode. In addition, blue circles highlight high intensities which are not present in the static phantom but appear in the cine and cardiac images. The black arrowhead shows intensities which reflect the blurring of the holes. R1 and R2 are the ROI's used for calculating CNR.

capturing motion of some joints. In addition, retro reconstructions need to be performed over the scanned cardiac phase on the CT's console after the cardiac images are obtained. This presents an extra step which can be time consuming especially in terms of driving a fully automated workflow. Nonetheless, this study showed the possibility to achieve dynamic scanning of a complete flexion extension motion of the knee by means of a cardiac scan mode at a low radiation exposure (0.02 mSv).

The predominant factors that impact the images obtained in 4D-CT MSK imaging are motion characteristics and the acquisition mode. Our findings emphasize the importance of speed of motion on the quality of images as is evident in the decline of image quality with an increase in hole speed. Motion artifacts were seen in the cine reconstructed images even when the fastest available gantry rotation speed (0.28 s) on the CT was used. The use of the cardiac mode with gantry rotation speed of 0.28 s on the other hand performed better with minimal artifacts.

In cardiac applications, acquiring quality images of coronary arteries is of prime importance, and as such these scan modes introduce techniques to minimize motion artifacts [30,31]. These techniques attempt to limit the angular coverage required to analytically reconstruct images and introduce iterative methods to reconstruct images with significantly lower motion artifacts [32,33]. For instance the intrinsic temporal resolution for the cardiac mode on the device used in this study is reported to be 0.14 s [34,35]. For the cine mode, a full (360°) CT rotation is required, i.e., 0.28 s. Following this initial 0.28 s, subsequent images can be reconstructed by using part of the data from the previous projection as long as a successive full 360° of projection data set is available. Other approaches used in cardiac scan mode are based on motion compensation, where a motion vector field that models cardiac motion is determined and used to compensate any motion during reconstruction [31,36]. Most CT vendors make use of variations of these techniques in their cardiac modes but not in conventional cine acquisitions. The exact implementation details used by manufacturers is often not documented or reported in literature. The results shown here are however, representative for the CT device used in this study. It will be of interest that such experiments can be tried on other devices to determine how valid these conclusions will be on other scanners from other manufacturers.

Regardless, our study highlights the benefit of making use of such a mode for dynamic MSK applications by quantitative measurements on phantom data and showing novel clinical data. As most CT's come with some form of a cardiac mode, this can offer radiologists and physicists the opportunity to investigate dynamic MSK phenomena with existing systems. We also expect that dynamic MSK studies will gain more clinical interest in the future due to the availability of wide-beam CT scanners today.

An important limitation of our study is that only uniplanar motion was considered in the phantom experiments. As motion artifacts can be influenced by the plane of the motion, further studies should be performed to investigate the influence of multiplanar motion on the image quality of these two scan modes. Despite that, the experiments on actual knee MSK data show that the conclusions drawn from the phantom experiments can be extended to more complex motions as is the case in flexion extension motion of the knee. Furthermore, our findings are based on a single CT device. Future experiments could compare these scan modes on other CT devices.

The 3D registration step introduced in the workflow for quantifying motion artifact was evaluated by visual inspection without any quantitative check for accuracy of this step. Even though visual inspection showed good alignment between static images and registered dynamic images, subtle misregistrations could be missed. Our workflow for motion artifact estimation focused on the volume regions of the artifacts, and not the severity of the intensity distortion. The entropy metric as proposed by Kyriakou et al. [37] could offer insights on intensity distorting motion artifacts. However, the estimation of motion from dynamic images is of importance in most MSK applications. Hence inaccuracies in localization of structures such as bones is of interest, since these can hinder the success of processing steps such as registration, rather than the presence of high intensities. The chosen metric was therefore sufficient to capture such volume and shape discrepancies and offer a good comparison between the two dynamic CT acquisition modes.

In conclusion, our study evaluated the impact of a cardiac CT scan mode on motion artifacts compared to a cine mode for the purpose of dynamic CT MSK studies. The quantitative motion artifact assessment showed that the cardiac acquisition mode showed significantly less motion artifacts in comparison to a cine mode acquisition. Results of the phantom study were consistent with scans of 3 knees of healthy volunteers obtained using the two modes. The findings of this study suggest that by using a cardiac acquisition mode, dynamic MSK images can be obtained with better quality to facilitate diagnosis and any onward image processing steps.

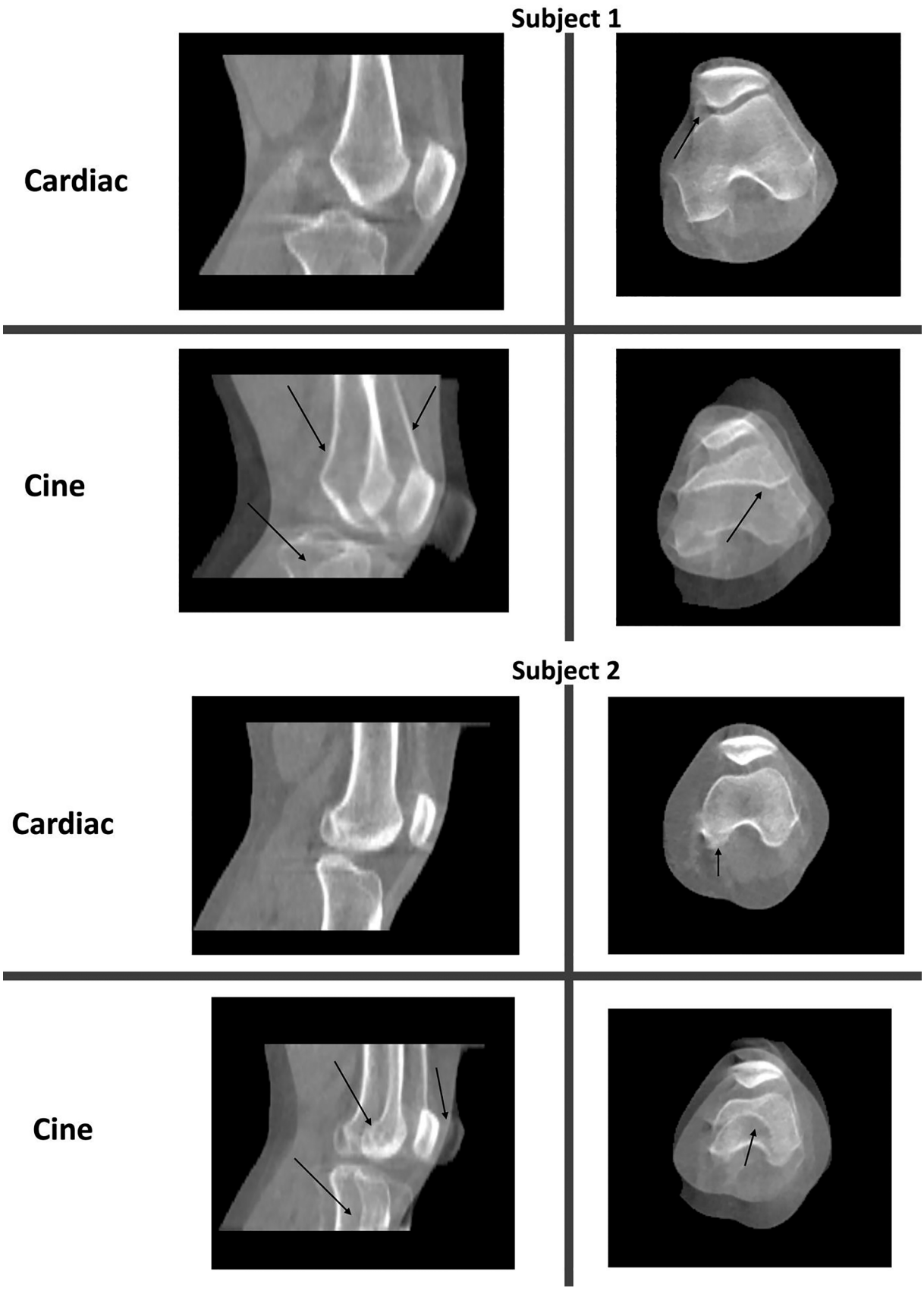

Fig. 9. Images of the knee undergoing motion for the three subjects in sagittal (left) and coronal (right) views obtained in cine and cardiac mode. Motion artifacts are predominant on the cine images as highlighted by the arrows.

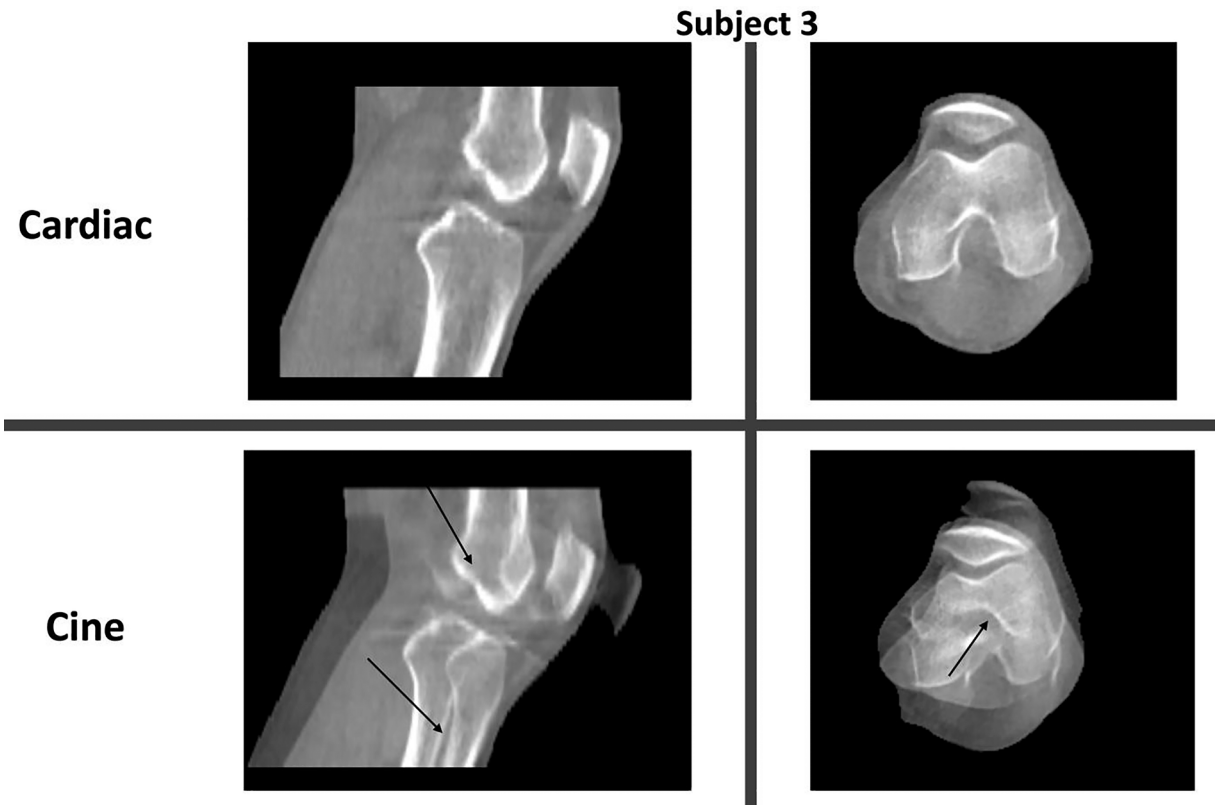

Fig. 9. (*continued*).

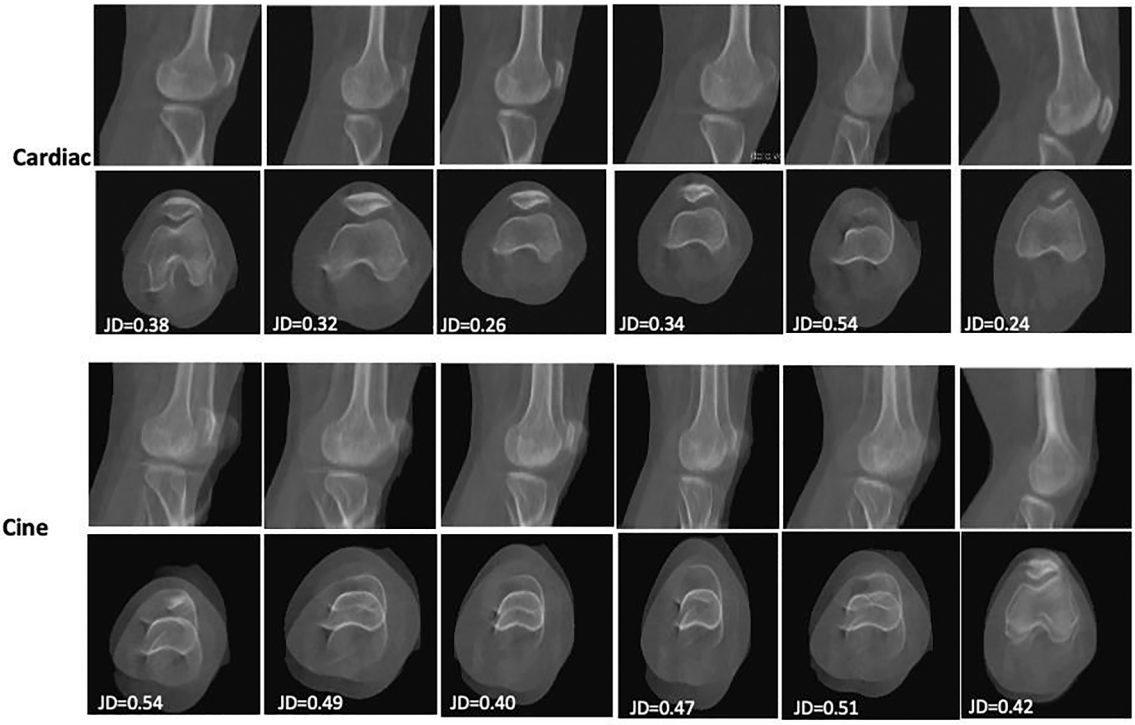

Fig. 10. Sagittal and axial slices from one of the subjects. The figure highlights the variation in motion artifacts at 6 consecutive time points for cardiac and cine scan modes. The Jaccard distances are shown as inserts on the axial images. The full dynamic sequence can be found in the supplementary data.

Funding

This research was funded by an Interdisciplinary Research Project grant (IRP KARMA-4D) from Vrije Universiteit Brussel.

Declaration of Competing Interest

The authors declare that they have no known competing financial interests or personal relationships that could have appeared to influence

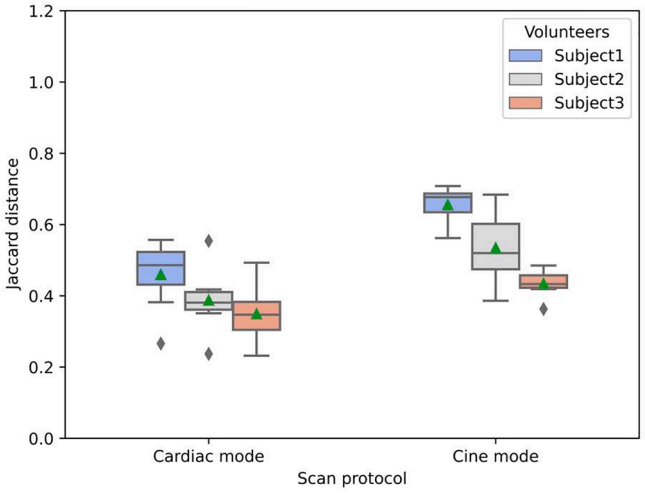

Fig. 11. Box plots showing the distribution of the Jaccard distance of the two dynamic CT acquisition modes for the three volunteers. Results shown are computed over all time points.

the work reported in this paper.

Appendix A. Supplementary data

Supplementary data to this article can be found online at https://doi.org/10.1016/j.ejmp.2022.10.028.

References

[1] Teixeira P, Gervaise A, Louis M, Raymond A, Formery A-S, Lecocq S, et al. Musculoskeletal wide-detector CT kinematic evaluation: from motion to image. Sem. Musculosk. Radiol. 2015;19(05):456–62.

[2] Tanaka MJ, Elias JJ, Williams AA, Carrino JA, Cosgarea AJ. Correlation between changes in tibial tuberosity-trochlear groove distance and patellar position during active knee extension on dynamic kinematic computed tomographic imaging. Arthroscopy 2015;31(9):1748–55. https://doi.org/10.1016/j.arthro.2015.03.015.

[3] Williams AA, Elias JJ, Tanaka MJ, Thawait GK, Demehri S, Carrino JA, et al. The relationship between tibial tuberosity-trochlear groove distance and abnormal patellar tracking in patients with unilateral patellar instability. Arthrosc. – J. Arthrosc. Relat. Surg. 2016;32(1):55–61.

[4] D'Agostino P, Dourthe B, Kerkhof F, Stockmans F, Vereecke EE. In vivo kinematics of the thumb during flexion and adduction motion: Evidence for a screw-home mechanism. J. Orthop. Res. 2017;35(7):1556–64. https://doi.org/10.1002/jor.23421.

[5] Wassilew GI, Janz V, Heller MO, Tohtz S, Rogalla P, Hein P, et al. Real time visualization of femoroacetabular impingement and subluxation using 320-slice computed tomography. J. Orthop. Res. 2013;31(2):275–81.

[6] Gondim Teixeira PA, Formery A-S, Jacquot A, Lux G, Loiret I, Perez M, et al. Quantitative analysis of subtalar joint motion with 4D CT: proof of concept with cadaveric and healthy subject evaluation. Am. J. Roentgenol. 2017;208(1):150–8.

[7] Buzzatti L, Keelson B, Apperloo J, Scheerlinck T, Baeyens J-P, Van Gompel G, et al. Four-dimensional CT as a valid approach to detect and quantify kinematic changes after selective ankle ligament sectioning. Sci. Rep. 2019;9(1). https://doi.org/10.1038/s41598-018-38101-5.

[8] Kerkhof FD, Brugman E, D'Agostino P, Dourthe B, van Lenthe GH, Stockmans F, et al. Quantifying thumb opposition kinematics using dynamic computed tomography. J. Biomech. 2016;49(9):1994–9.

[9] Forsberg D, Lindblom M, Quick P, Gauffin H. Quantitative analysis of the patellofemoral motion pattern using semi-automatic processing of 4D CT data. Int. J. Comput. Assist. Radiol. Surg. 2016;11(9):1731–41. https://doi.org/10.1007/s11548-016-1357-8.

[10] Leng S, Zhao K, Qu M, An K-N, Berger R, McCollough CH. Dynamic CT technique for assessment of wrist joint instabilities. Med. Phys. 2011;38(Suppl 1):S50. https://doi.org/10.1118/1.3577759.

[11] Neo PY, Mat Jais IS, Panknin C, Lau CC, Chan LP, An KN, et al. Dynamic imaging with dual-source gated Computed Tomography (CT): implications of motion parameters on image quality for wrist imaging. Med. Eng. Phys. 2013;35(12):1837–42.

[12] Keelson B, Buzzatti L, Ceranka J, Gutiérrez A, Battista S, Scheerlinck T, et al. Automated motion analysis of bony joint structures from dynamic computer tomography images: a multi-atlas approach. Diagnostics (Basel, Switzerland) 2021;11(11):2062.

[13] Gondim Teixeira PA, Formery A-S, Hossu G, Winninger D, Batch T, Gervaise A, et al. Evidence-based recommendations for musculoskeletal kinematic 4D-CT studies using wide area-detector scanners: a phantom study with cadaveric correlation. Eur. Radiol. 2017;27(2):437–46.

[14] Chen G-H, Tang J, Hsieh J. Temporal resolution improvement using PICCS in MDCT cardiac imaging. Med. Phys. 2009;36(6Part1):2130–5.

[15] Taguchi K. Temporal resolution and the evaluation of candidate algorithms for four-dimensional CT. Med. Phys. 2003;30(4):640–50.

[16] Apfaltrer P, Schoendube H, Schoepf UJ, Allmendinger T, Tricarico F, Schindler A, et al. Enhanced temporal resolution at cardiac CT with a novel CT image reconstruction algorithm: Initial patient experience. Eur. J. Radiol. 2013;82(2):270–4.

[17] B. Keelson *et al.*, "Quantifying motion artifacts using a rotating phantom: insights towards dynamic musculoskeletal applications," *https://doi.org/10.1117/12.2542159*, vol. 11312, pp. 710–717, Mar. 2020, doi: 10.1117/12.2542159.

[18] Raj R, Sivanandan KS. Elbow joint angle and elbow movement velocity estimation using NARX-multiple layer perceptron neural network model with surface EMG time domain parameters. J. Back Musculosk. Rehabil. 2017;30(3):515–25.

[19] Mentiplay BF, Banky M, Clark RA, Kahn MB, Williams G. Lower limb angular velocity during walking at various speeds. Gait Posture 2018;65:190–6.

[20] Yaniv Z, Lowekamp BC, Johnson HJ, Beare R. SimpleITK image-analysis notebooks: a collaborative environment for education and reproducible research. J. Digit. Imaging 2018;31(3):290–303.

[21] Warren C, Hamarneh G. N-sift: N-dimensional scale invariant feature transform for matching medical images. In: 2007 4th IEEE International Symposium on Biomedical Imaging: From Nano to Macro - Proceedings; 2007. p. 720–3. https://doi.org/10.1109/ISBI.2007.356953.

[22] "Insight Journal (ISSN 2327-770X) - Introducing Dice, Jaccard, and Other Label Overlap Measures To ITK." https://www.insight-journal.org/browse/publication/707 (accessed May 25, 2021).

[23] Shapiro SS, Wilk MB. An analysis of variance test for normality (Complete Samples). Biometrika Dec. 1965;52(3/4):591. https://doi.org/10.2307/2333709.

[24] Williams WA, Snedecor GW, Cochran WG, Cox DF. Statistical methods. J. Am. Stat. Assoc. 1991;86(415):834. Accessed: May 25, 2021. [Online]. Available: https://go.gale.com/ps/i.do?p=AONE&sw=w&issn=01621459&v=2.1&it=r&id=GALE%7CA257786252&sid=googleScholar&linkaccess=fulltext.

[25] Lee C, Kim KP, Bolch WE, Moroz BE, Folio L. NCICT: a computational solution to estimate organ doses for pediatric and adult patients undergoing CT scans. J. Radiol. Prot. 2015;35(4):891–909.

[26] Fat DL, Kennedy J, Galvin R, O'Brien F, Grath FM, Mullett H. The Hounsfield value for cortical bone geometry in the proximal humerus-an in vitro study. Skeletal Radiol. May 2012;41(5):557–68. https://doi.org/10.1007/S00256-011-1255-7.

[27] P. O. Østbyhaug, J. Klaksvik, P. Romundstad, A. Aamodt, P. Østbyhaug, and O. Surgeon, "human femora with anatomical and customised femoral stems," pp. 91–676, 2009, doi: 10.1302/0301-620X.91B5.

[28] Jibri Z, Jamieson P, Rakhra KS, Sampaio ML, Dervin G. Patellar maltracking: an update on the diagnosis and treatment strategies. Insights Imaging 2019;10(1):Dec. https://doi.org/10.1186/S13244-019-0755-1.

[29] Garcia-Elias M. The non-dissociative clunking wrist: A personal view. J. Hand Surg. Eur. 2008;33(6):698–711. https://doi.org/10.1177/1753193408090148.

[30] M. Jin, C. Zhao, X. Jia, and L. Yu, "Motion-compensated reconstruction for limited-angle multiphase cardiac CT," *https://doi.org/10.1117/12.2294922*, vol. 10573, pp. 796–803, Mar. 2018, doi: 10.1117/12.2294922.

[31] Hahn J, Bruder H, Rohkohl C, Allmendinger T, Stierstorfer K, Flohr T, et al. Motion compensation in the region of the coronary arteries based on partial angle reconstructions from short-scan CT data. Med. Phys. 2017;44(11):5795–813.

[32] Reports M-K-C-C-I, undefined,. Iterative reconstruction techniques: What do they mean for cardiac CT? Springer 2013. https://doi.org/10.1007/s12410-013-9203-7.

[33] Tang J, Hsieh J, Chen G-H. Temporal resolution improvement in cardiac CT using PICCS (TRI-PICCS): performance studies. Med. Phys. 2010;37(8):4377–88.

[34] Hong SH, Goo HW, Maeda E, Choo KS, Tsai IC. User-friendly vendor-specific guideline for pediatric cardiothoracic computed tomography provided by the Asian society of cardiovascular imaging congenital heart disease study group: Part 1. imaging techniques. Korean J Radiol 2019;20(2):190–204. https://doi.org/10.3348/KJR.2018.0571.

[35] Lewis MA, Pascoal A, Keevil SF, Lewis CA. Selecting a CT scanner for cardiac imaging: the heart of the matter. Br. J. Radiol. 2016;89(1065):20160376.

[36] Maier J, Lebedev S, Erath J, Eulig E, Sawall S, Fournié E, et al. Deep learning-based coronary artery motion estimation and compensation for short-scan cardiac CT. Med. Phys. 2021;48(7):3559–71.

[37] Kyriakou Y, Lapp RM, Hillebrand L, Ertel D, Kalender WA. Simultaneous misalignment correction for approximate circular cone-beam computed tomography. iopscienceioporg 2008;53(22):6267–89.